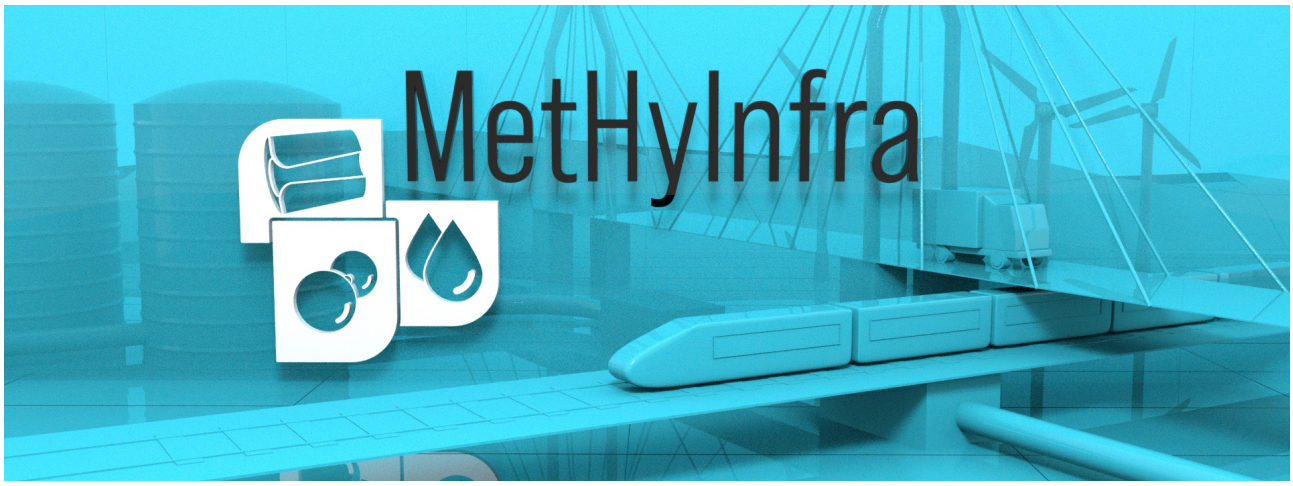

REPORT: Uncertainty in U-shape Coriolis mass flow meter for liquid hydrogen measurements

A4.3.5

Authors: Federica Gugole, Dean Standiford, Jože Kutin, Oliver Büker

Confidentiality: Public

Submission date: 28.10.2022

Revision: 2.2

methyinfra.ptb.de

Report A4.3.5	
Funding European Metrology Program for Innovation and Research	**Grant agreement no:** 20IND11
Project name Metrology infrastructure for high-pressure gas and liquified hydrogen flows	**Project short name** MetHyInfra
Author(s)	**Pages**

Federica Gugole	VSL	fgugole@vsl.nl
Dean Standiford	VSL	dstandiford@vsl.nl
Jože Kutin	UL	joze.kutin@fs.uni-lj.si
Oliver Büker	RISE	oliver.buker@ri.se

16 pages

Summary

This report was written as part of activity 4.3.5 from the EMPIR Metrology infrastructure for high-pressure gas and liquified hydrogen flows (MetHyInfra) project. The three-year European project commenced on 1st June 2021 and focused on providing metrological infrastructure and traceability for high pressure hydrogen flow meter calibration (1000 bar / 3.6 kg/min), fuel cells applications (4 kg/h, 30 bar) and liquid hydrogen. For more details about this project please visit methyinfra.ptb.de.

Confidentiality	Public

This project (20IND11 MetHyInfra) has received funding from the EMPIR programme co-financed by the Participating States and from the European Union's Horizon 2020 research and innovation programme.

The EMPIR initiative is co-funded by the European Union's Horizon 2020 research and innovation programme and the EMPIR Participating States

Contents

List of Figures

List of Tables

Summary

We reviewed the available literature on Coriolis mass flow meter (CMF) measurements and the associated uncertainty in order to obtain an uncertainty budget for a CMF calibrated with water but used to measure liquid hydrogen.

We consider here two (physics based) equations of the mass flow rate through a CMF: the first equation was derived by [Raszillier and Durst, 1991] for a straight tube design, and the second was inferred by [Costa et al., 2020] for a U-shape design. [Wang and Hussain, 2009] compared the results of the equation by Raszillier and Durst (1) to the outcomes of a finite element analysis of a CMF with two parallel U-shape stainless steel 316 tubes at different temperatures. The comparison found small deviations, thus concluding that equation (1) is applicable to measuring tubes with complicated geometrical features. We did not find any study comparing the equation from Costa et al (2) to the outcomes of a numerical model, thus equation (2) still needs to be validated for CMF of different shapes. The application of both equations for the quantification of the measurement uncertainty of delta-shape meters requires prior validation of the equations for such a shape of the CMF.

We also checked which phenomena affect the readings of CMFs. On this regard we found that temperature has a strong influence on the meter readings since it affects the thermal expansion of the meter geometry and the elastic properties of the stainless steel, which have a nonlinear behavior at cryogenic temperatures. At the time of writing there was only one publicly available dataset on measurements of the elastic properties of stainless steel 304, 310 and 316. This dataset was reported by [Ledbetter, 1981]. However the uncertainties associated with these measurements are rather large ($1 - 2$ %) depending on the quantity and on the steel) and badly reported (the data were published before the first draft of the GUM had been released). [Ledbetter et al., 1980] reports two uncertainty sources (i.e., repeatability and lot-to-lot variability) for stainless steel 304. By assuming that the uncertainty budgets for stainless steel 316 has been obtained in the same manner as for stainless steel 304, and assuming that the repeatability reported for stainless steel 304 is valid also for stainless steel 316, the uncertainty in the Young's modulus and Poisson's ratio can be reduced to 0.5 %. However, given the pieces of information reported in the literature, it is not possible to verify if these assumptions hold.

Several studies have been performed to determine the effect of pressure on CMF measurements. Quite some studies (e.g., [Mills, 2020, Costa et al., 2020]) revealed pressure correction factors in line with the pressure correction coefficients declared by manufacturers [Kuhny, 2011]. Hence we used the pressure correction factor declared by Emerson© as a proxy to be employed in the calculation of the total uncertainty budget.

Often when performing this kind of uncertainty budget estimation, it is assumed that the fluid is in sub-cooled conditions, see e.g. [Wu et al., 2021, Wu and Kenbar, 2022]. However in the case of some liquid hydrogen measurement applications, boil-off is rather likely to happen and its effect on the measurements is therefore more relevant. The effect of measuring a two-phase, as opposed to a single-phase fluid is still a topic of active research. There are some theoretical estimation of the error induced by measuring a two-phase fluid (see [Hemp and Kutin, 2006, Basse, 2014]) but we did not find any measurement data that could validate such estimates. Therefore, we limit our uncertainty budget to the case of single-phase measurements and point out that further studies are needed to quantify the effect of measuring liquid hydrogen in the presence of boil-off.

The uncertainty contribution due to zero-point stability and repeatability depends on several factors, including

the facility where the measurements are performed. Since there are no data regarding the zero stability and repeatability of a CMF measuring the flow of liquid hydrogen, we assumed that the CMF at liquid hydrogen temperatures has a similar behaviour as at liquid natural gas or liquid nitrogen temperatures. Thus we used as proxies for these contributions their respective equivalent as measured by a CMF of similar shape tested with liquid natural gas and liquid nitrogen. However these assumptions should be checked and a careful quantification of the zero stability and repeatability should be performed for liquid hydrogen applications.

[Huber et al., 2013] showed that CMF measurements have a dependency on the Reynolds number particularly evident at low Reynolds numbers. They also note that a proper compensation can be performed by measuring the viscosity of the fluid, however this should not be an issue at typical Reynolds number values for liquid hydrogen flows.

Numerical studies by [Bobovnik et al., 2015] and [Kutin et al., 2006] aimed at quantifying installation and velocity profile effects on the CMF measurements. [Bobovnik et al., 2015] reported a $0.1\ \%$ installation effect, however they also note that the actual value of the installation effect for any configuration depends on the design features of the CMF. We decided therefore not to include this contribution to the total uncertainty budget, since it appears to be valid only for few specific cases and because of the lack of data that could be used to validate such estimate. However we advice users to take care when installing the meter, and to perform tests (if possible) in order to assess the installation effect for their specific case. [Kutin et al., 2006] states that the magnitude of velocity profile effects is dependent on the design of the CMF. This effect is also very difficult to generalize and thus it is not considered in the uncertainty budget.

We combined the aforementioned uncertainty contributions according to the *Guide to the expression of uncertainty in measurement* (GUM) [BIPM, 2008a] and obtained a standard uncertainty of $0.50\ \%$ (k=1) for equation (1) and of $0.56\ \%$ (k=1) for equation (2). These budgets are strongly dominated by the uncertainty in the measurements of the elastic properties of stainless steel 316, i.e., $u_E = 0.5\ \%$ (k=1) for the Young's modulus and $u_\nu = 0.5\ \%$ (k=1) for the Poisson's ratio. However, the uncertainty of the elastic properties of stainless steel are calibrated out at ambient conditions and only the uncertainty at cryogenic temperatures and any measurement correlations need to be considered. Therefore, to achieve a lower uncertainty budget, the priority should be on improving the measurements and associated uncertainties of the elastic properties of stainless steel at cryogenic temperatures.

1 Equations for CMF measurements

1.1 Equation for a straight tube CMF

[Raszillier and Durst, 1991] developed a simplified model for the mass flow rate measured by a Coriolis mass flow meter (CMF) with a straight tube design and without axial stresses. [Wang and Hussain, 2009] compared the results of this equation to the outcomes of a finite element analysis of a CMF with two parallel U-shape stainless steel 316 tubes at different temperatures. The comparison found small deviations, thus concluding that equation (1) is applicable to measuring tubes with complicated geometrical features. The equation reads:

$$Q_m = \frac{C}{\gamma\left(\frac{x_L}{L_p}\right) L_p^3} E(T) I_p \Delta t = FCF\Delta t \tag{1}$$

where

- Q_m is the mass flow rate;
- $E(T)$ is the Young's modulus as a function of the temperature T;
- $I_p = \pi \left(r_o^4 - r_i^4\right)/4$ is the moment of inertia of the pipe;
- r_o and r_i are the outer and inner radii of the pipe, respectively;
- C is a constant;
- $\gamma\left(\frac{x_L}{L_p}\right)$ is a function of the sensor location x_L in relation to the length of the pipe L_p; both $\frac{x_L}{L_p}$ and $\gamma\left(\frac{x_L}{L_p}\right)$ can be treated as constants;
- Δt is the time delay detected by the two sensors on the tube;
- FCF stands for flow calibration factor.

Since we are interested in the relative changes when the CMF is used to measure the flow of liquid hydrogen but it has been calibrated with water at ambient temperatures, we investigate only uncertainties related to the flow calibration factor and neglect uncertainties in Δt.

1.2 Equation for a U-shape CMF

[Costa et al., 2020] derived an equation for the mass flow rate measured by a U-shape CMF.

$$Q_m = \frac{3\pi E\left(T\right)\left(r_o^4 - r_i^4\right)}{32SL^3}\left[1 + \frac{4L^2}{3W^2\left(\nu\left(T\right)+1\right)} - \frac{\pi\beta_1^4 W}{12L}\right]\Delta t = FCF\Delta t \tag{2}$$

where:

- S is a dimensionless shape parameter;
- L is the length of the flow tubes plus the U bend radius;
- W is the distance between the inlet and the outlet tube segments;
- $\nu(T)$ is the Poisson's ratio expressed as a function of the temperature T;
- $\beta_1 \approx 1.8751$ is the first order solution to the cantilever beam mathematical model.

2 Compensations due to temperature

Temperature changes affect the elastic properties of the steel and the geometric dimensions of the meter. In order to keep this into account in the uncertainty budget, we shall apply a temperature correction for the Young's modulus and Poisson's ratio. Furthermore we shall consider the linear thermal expansion coefficient in the geometric dimensions of the meter.

2.1 Young's modulus and Poisson's ratio

[Ledbetter, 1981] provides measurement data of the Young's modulus and Poisson ratio for stainless steel 304, 310 and 316 at temperatures between 5 K and 295 K. The measurements have been obtained using longitudinal and transverse ultrasonic velocities. The associated uncertainties have been reported in [Ledbetter et al., 1980] in case of stainless steel 304, and in [Ledbetter, 1980] for the cases of stainless steel 310 and 316. It has to be noted that these three papers have been published before the publication of the first version of the *Guide to the expression of uncertainty in measurement* (GUM) [BIPM, 2008a], therefore the notation used there is not to be interpreted using the current conventions. After careful reading and reproduction of (some of) the calculations, it has been concluded that the uncertainty estimates reported in [Ledbetter et al., 1980] and [Ledbetter, 1980] are standard uncertainties (i.e. $k = 1$). In case of stainless steel 316, [Ledbetter, 1980] reports standard uncertainty of $1.9\,\%$ and of $0.9\,\%$ for the Young's modulus and Poisson's ratio, respectively (see Table 3 in [Ledbetter, 1980]).

It has to be noted that the uncertainties reported by [Ledbetter, 1980] (and [Ledbetter et al., 1980]) might not be realistic anymore. The values reported in [Ledbetter, 1980] include any source of uncertainty such as chemical composition, thermomechanical processing and sample anisotropy. However, since 1980, there have been quite some technological developments in the manufacturing industry, thus it is reasonable to assume that the individual uncertainty contributions of the components considered by [Ledbetter, 1980] might have changed. Furthermore, since the CMF used to measure the hydrogen flow is calibrated at ambient temperatures, some of the uncertainty components (e.g., lot-to-lot variability and uncertainty in the density of the material) may be excluded. Unfortunately, the estimates of some of the different uncertainty contributions (i.e., repeatability and lot-to-lot variability) are provided only for stainless steel 304 [Ledbetter et al., 1980], and no information is available to extend the estimate of these uncertainty components to stainless steel 316. As a final comment on this topic, we note that the uncertainty budget has been provided for $T = 295$ K [Ledbetter, 1980] and it is unclear how these estimates apply at cryogenic temperatures.

For the uncertainty budget reported here, we rely on the measurements by [Ledbetter, 1981] and their associated uncertainties. Since the measurements for stainless steel 316 have likely been performed in the same facility, following the same procedure (by the same operators) as the measurements for stainless steel 304, it could be assumed that the repeatability component reported by [Ledbetter et al., 1980] (or a similar value) is valid also for stainless steel 316. On this regard we note that the total uncertainty budget for stainless steel 304 reported by [Ledbetter et al., 1980] is the result of the squared sum of the repeatability and the lot-to-lot variability components. If we assume that the uncertainty budget for stainless steel 316 has been built in the same fashion (i.e., squared sum of the repeatability and the lot-to-lot variability), we could consider only the repeatability component since the lot-to-lot variability is calibrated out at ambient temperature. We remark that these are assumptions and that the pieces of information reported in the literature are not sufficient to verify if these assumptions hold or not. In this report we will work with these underlining assumptions and consider only the repeatability component in the uncertainty budget for the elastic properties of stainless steel 316. The standard uncertainty due to repeatability reported by [Ledbetter et al., 1980] amounts to $0.5\,\%$ both for the Young's modulus and for the Poisson's ratio.

2.1.1 Uncertainty of the corrected elastic properties

Both in equation (1) and in equation (2) we have $\Delta Q_m \propto \Delta E$. Thus the relative error in Q_m due to the relative

error in E can be defined as

$$\frac{\Delta Q_m}{Q_m} = \frac{\Delta E}{E}$$

and the relative standard uncertainty in Q_m due to the relative error in the Young's modulus is estimated as $u_E = 0.5\,\%$.

Equation (1) does not depend on the Poisson's ratio, while in equation (2) we have $Q_m \propto 1/(\nu + 1)$. An analytical approach to quantify the uncertainty contribution of ν in equation (2) would require the calculation of the partial derivative with respect to ν and of its associated sensitivity coefficient. Since the equation is relatively complex, it is quite easy to make mistakes when calculating the partial derivative and of the sensitivity coefficient. Thus we prefer to adopt an approach based on the Monte Carlo method [BIPM, 2008b] to estimate the temperature related uncertainty budget of equation (2).

An alternative approach would be to notice that $FCF \propto E$ and write

$$FCF(T) = FCF(T_0)\frac{E(T)}{E(T_0)}\,,$$

where T_0 is the temperature at which the meter has been calibrated. This expression shows that only the uncertainties due to the change of E as a function of the temperature are important (and measurement correlations if present). However, this piece of information is not available for the measurement by [Ledbetter, 1981], so in the current study we use the repeatability uncertainty contribution reported by [Ledbetter et al., 1980] and note that if more information become available in the future, then the uncertainties related to the elastic properties of the steel can be reduced to those stemming from the temperature dependence and the measurement correlations.

2.1.2 Temperature measurement effect on Young's modulus and on Poisson's ratio

Measurement data at VSL's LNG facility show a maximum error in temperature measurements of 3 K in case of insulated meters, and of 7 K in case of non-insulated flow meters. We assume that such errors in the temperature measurements apply also to liquid hydrogen. The meters used in the MetHyInfra project are insulated, therefore here we analyze the case of insulated meters and leave the case of non-insulated meters to a later study. A maximum error in temperature measurements of 3 K at a nominal temperature $T = 20$ K causes a maximum error of $0.073\,\%$ and of $0.020\,\%$ in Young's modulus and Poisson's ratio respectively. Thus the standard uncertainty for the Young's modulus due to temperature measurement error is $u_{t,E} = 0.073\,\%/\sqrt{3} \approx 0.042\,\%$ assuming a uniform distribution. A similar computation can nominally be computed also for the Poisson's ratio, however as mentioned above, we prefer to assess the uncertainty budget of equation (2) (which considers the Poisson's ratio) using the Monte Carlo method.

2.2 Linear thermal expansion

Temperature has an important effect also on the geometry of the meter itself. As the temperature increases (decreases), the steel expands (shrinks) thus modifying the geometric parameters of the meter. The thermal expansion of the material of the flow meter is usually modelled as a percentage linear expansion which, for stainless steel 316 in the temperature range 4-293 K, is given by [NIST, 2017] as

$$\frac{l(T) - l(T_{ref})}{l(T_{ref})} = \alpha - 1 = \begin{cases} 10^{-5} \cdot (a + bT + cT^2 + dT^3 + eT^4)\,, & \text{if } T \geq 23\text{ K} \\ 10^{-5} \cdot f\,, & \text{if } T < 23\text{ K} \end{cases} \tag{3}$$

where $l(T)$ stands for any length dimension dependent on temperature, $a = -295.54$, $b = -.39811$, $c = 9.2683E-3$, $d = -2.0261E-5$, $e = 1.7127E-8$ and $f = -300.04$. Note that according to equation (3) there is no temperature dependency in the thermal expansion coefficient for temperature lower than 23 K. The values of α given by equation (3) are plotted in figure 1. [Desai and Y., 1978] reported the recommended values for the thermal expansion coefficient and reports an uncertainty of $5\ \%$. It is not specified whether this is a standard $(k = 1)$ or expanded $(k = 2)$ uncertainty. In the following calculations it is assumed that it is an expanded uncertainty and that it applies also to the polynomial fit.

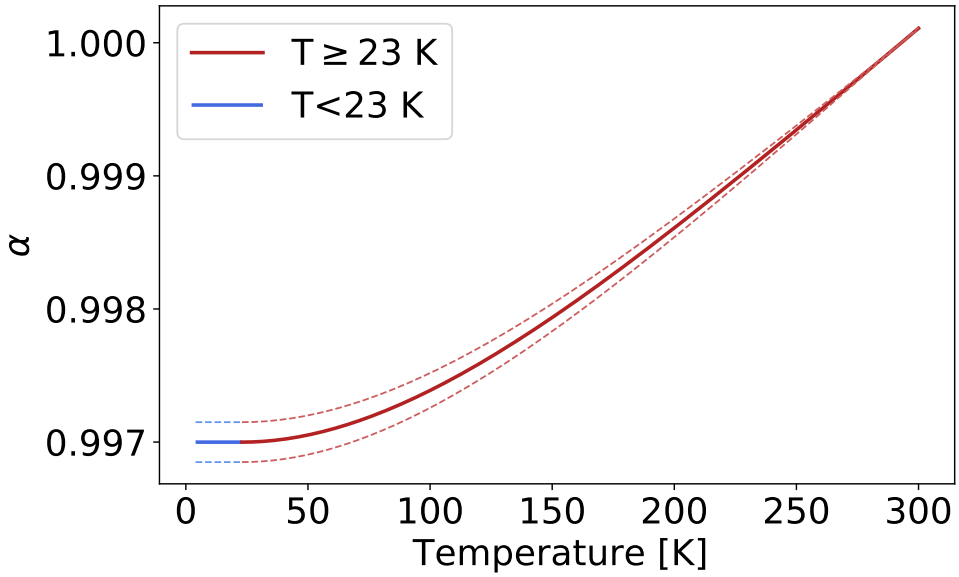

Figure 1: NIST polynomial fit for the thermal expansion coefficient α for stainless steel 316. The dashed lines denote the $95\ \%$ confidence interval (assuming a normal distribution and $U_{1-\alpha}(k = 2) = 5\ \%$) associated to equation (3).

It is generally assumed that tube length, inner and outer radii, and any other geometry related quantity expand following equation (3), see, e.g., [Wu et al., 2021, Wu and Kenbar, 2022]. Thus we have $L_p(T) = \alpha L_p(T_{ref})$, $L(T) = \alpha L(T_{ref})$, $r_o(T) = \alpha r_o(T_{ref})$ and $r_i(T) = \alpha r_i(T_{ref})$. At $T = 20$ K the mean value of α is 0.99696, and its expanded uncertainty is 0.00015 $(k = 2)$. Hence the relative expanded uncertainty associated to α is $U_\alpha(k = 2) = 0.015\ \%$.

After correction of the tube thermal expansion, equation (1) can be rewritten as

$$Q_m = \frac{C\pi\alpha^4\left(r_o^4 - r_i^4\right)}{4\gamma\left(\frac{\alpha x_L}{\alpha L_p}\right)\alpha^3 L_p^3}E(T)\Delta t = \frac{C\pi\alpha\left(r_o^4 - r_i^4\right)}{4\gamma\left(\frac{x_L}{L_p}\right)L_p^3}E(T)\Delta t\,, \tag{4}$$

and equation (2) as

$$\begin{aligned} Q_m &= \frac{3\pi E\left(T\right)\alpha^4\left(r_o^4 - r_i^4\right)}{32S\alpha^3 L^3}\left[1 + \frac{4\alpha^2 L^2}{3\alpha^2 W^2\left(\nu\left(T\right)+1\right)} - \frac{\pi\beta_1^4\alpha W}{12\alpha L}\right]\Delta t \\ &= \frac{3\pi E\left(T\right)\alpha\left(r_o^4 - r_i^4\right)}{32SL^3}\left[1 + \frac{4L^2}{3W^2\left(\nu\left(T\right)+1\right)} - \frac{\pi\beta_1^4 W}{12L}\right]\Delta t\,. \end{aligned} \tag{5}$$

In both equations we have that Q_m is directly proportional to α, thus variations in Q_m are also directly proportional to variations in α: $\Delta Q_m \propto \Delta\alpha$. Therefore the relative error in Q_m caused by the relative error in α can be related as

$$\frac{\Delta Q_m}{Q_m} = \frac{\Delta\alpha}{\alpha}$$

and the relative standard uncertainty in Q_m caused by the relative error in α is estimated as $u_\alpha = U_\alpha/2 = 0.015\ \%/2 \approx 0.008\ \%$, assuming a normal distribution.

2.2.1 Temperature measurement effect on thermal expansion

As discussed in the previous paragraph, a relative error in α causes the same relative error in the mass flow rate measurement. According to equation (3) given by [NIST, 2017], the thermal expansion coefficient is constant for $T < 23$ K. This means that if the liquid hydrogen being measured is at a nominal temperature of 20 K, errors up to 3 K in the temperature measurement do not further contribute to the total measurement uncertainty. Thus, assuming a nominal temperature of 20 K and a maximum error of 3 K in the temperature measurement, there is no further contribution to the total uncertainty budget related to the thermal expansion.

3 Compensations due to pressure

When fluid pressure increases, the CMF's tube gets stiffer affecting the mass flowrate measurement. It is well known that the pressure dependence is larger for larger flow meters, while it is negligible (for most applications) in case of small flow meters [Kuhny, 2011]. [Mills, 2020] reported a linear effect due to pressure and, just as [Costa et al., 2020], found a correction factor matching the manufacturer's specifications. In a like manner [Wang and Hussain, 2010] found a difference between theoretical and experimental data. However also in this case the pressure sensitivity coefficient found is in general agreement with the manufacturer's specification. Furthermore, [Wang and Hussain, 2010] noted that the newer generation of CMF have a reduced pressure sensitivity with respect to the meters of the previous generation. Finally, [Büker et al., 2020] did not find any pressure dependency when testing small size CMFs in a high-pressure facility.

The overall conclusion is therefore that the pressure correction term expressed by manufacturers is reliable and its uncertainty can thus be taken as the pressure related uncertainty contribution to the total uncertainty budget. If the pressure correction is not applied to the measurement result, based on the specification of a commercial delta-shape CMF100 and of a U-shape CMF200 [Emerson, 2021] an expanded uncertainty in the pressure correction factor is $c_p = -0.003\ \%$/bar and $c_p = -0.009\ \%$/bar for the delta shape and U-shape respectively. Assuming an operating liquid hydrogen pressure of 7 barg and a calibration pressure of 1 barg, then the expanded uncertainty from pressure correction is derived as $U_p = |6c_p| = 0.018\ \%$ for the delta-shape CMF and as $U_p = |6c_p| = 0.054\ \%$ for the U-shape CMF. The standard uncertainty is thus $u_p = U_p/2 = 0.009\ \%$ for CMF100 and $u_p = U_p/2 = 0.027\ \%$ for CMF200, assuming a normal distribution. We remark that in this derivation the pressure measurement uncertainty and the pressure drop across the CMF are assumed negligible. If instead the actual pressure correction is applied, the uncertainty due to pressure is reduced to the uncertainty in the pressure correction factor and the uncertainty in the pressure measurements.

We note that both equation (1) and equation (2) do not have an explicit dependence on pressure. Thus, in case

of an uncertainty budget obtained via Monte Carlo, the uncertainty component due to pressure needs to be added to the result of the Monte Carlo simulations. It is assumed that this error contribution is independent from the results of the equations.

4 Compensations due to two-phase fluid

Unlike other cryogenic fluids, in some liquid hydrogen measurement applications it is not that unlikely to have a two-phase fluid (i.e., liquid and gaseous hydrogen) since boil-off may happen more easily than in case of other cryogenic fluids. As an example, in stationary liquid hydrogen storage the boil-off rate due to heat transferred from the surroundings varies with the volume of the storage tank, with the boil-off rate increasing above $1\,\%$ in case of small tanks [Aziz, 2021]. However highly effective cooling systems with very low boil-off rates are being studied and proposed, see for instance the cooling system presented by [Xu et al., 2020]. In those cases where significant boil-off takes place, corrections to the measurement result should be considered to account for the error caused by measuring a two-phase fluid. This error is due to combinations of complex physical effects such as inertia, damping and compressibility, and there is no unified analytical correction for these effects.

In the light of these research studies, we decided to assume a situation where boil-off is negligible (compared to the other sources of uncertainties) for the calculation of the uncertainty budget. Nonetheless, for sake of completeness, we report here the main findings regarding errors due to two-phase fluids measurements and we note that the corresponding measurement error can be considered to be independent from the other uncertainty sources, and it can thus be easily added to the uncertainty budget here estimated. Finally, it should be noted that we did not find any data that could be used to validate the error estimates due to two-phase fluid.

4.1 Hemp and Kutin

[Hemp and Kutin, 2006] calculated the fractional error E_d in fluid density measurement and the fractional error E_{Q_m} in mass flow reading due to the compressibility of the fluid as

$$E_d = -3\gamma + \frac{1}{4}\left(\frac{\omega_1}{c} r_i\right)^2 \qquad E_{Q_m} = -\frac{2\gamma}{1-\gamma} + \frac{1}{2}\left(\frac{\omega_1}{c} r_i\right)^2 \tag{6}$$

where

- γ is the gas volume fraction;
- ω_1 is the actual resonance frequency of vibration;
- c is the speed of sound in the two-phase fluid.

The main assumptions considered in the development of equation (6) are:

- the resonance frequency of transverse fluid vibrations f_i is much larger than the frequency of operation of a CMF f_1, i.e. $f_i >> f_1$;
- bubbles are uniformly distributed within the flow meter;

- errors due to the relative motion of the bubbles and liquid are negligible.

Furthermore the calculation of E_{Q_m} has been performed only for a straight tube and for the case of a flat flow velocity profile. Damping effects in two-phase fluids in vibrating tubes have not been investigated.

4.2 Basse

[Basse, 2014] presented a theoretical generalization of equations (6) for a general two-phase fluid (i.e., both for the liquid-gas and the liquid-solid combinations):

$$E_d = \frac{\gamma\left(\rho_f - \rho_p\right)\left(1-F\right)}{\gamma\rho_p + \left(1-\gamma\right)\rho_f} + \frac{1}{4}\left(\frac{\omega}{c}r_i\right)^2 \qquad E_{Q_m} = \frac{\gamma\left(\rho_f - \rho_p\right)\left(1-F\right)}{\gamma\rho_p + \left(1-\gamma\right)\rho_f} + \frac{1}{2}\left(\frac{\omega}{c}r_i\right)^2 \tag{7}$$

where

- ω is the driver frequency;
- $F = 1 + \frac{4(1-\tau)}{4\tau - \frac{9iG}{\beta^2}}$ is the reaction force coefficient;
- ρ_f is the density of the continuous fluid (in our case, liquid hydrogen);
- ρ_p is the density of the entrained particles (in our case, bubbles of gaseous hydrogen).

However from Basse's paper [Basse, 2014] it is not clear to us which assumptions have been used to derive equation (7).

4.2.1 Damping effects in two-phase fluids

[Basse, 2016] derived the work done per cycle on the entrained particles

$$W_p = \pi\left(\rho_f - \rho_p\right)\gamma V_{f-p}\Omega^2 + \mathrm{Im}(F)\overline{u^2} \tag{8}$$

where

- $V_{f-p} = V_f + V_p$ is total volume of the two-phase fluid;
- Ω is the angular frequency;
- $\overline{u^2}$ is the mean deflection squared
- $\gamma = \frac{V_p}{V_p + V_f}$ is the volumetric particle fraction;

In the examples analyzed by [Basse, 2016], the temperature increase due to the drag between the fluid and the entrained particles is negligible.

4.3 Comparison with experimental data

[Anklin et al., 2000] used experimental data for straight tube CMF with nominal diameters ranging between 25 mm and 100 mm and found deviations due to the speed of sound of the fluid and fluid velocity proportional to $(2\pi\omega_1 d/c)^2$ where d is the diameter of the tube and c is the speed of sound of the fluid. This shows that considering an error proportional to the square of the resonant frequency works well for practical purposes, however the question remains regarding which correction is more appropriate and how this generalizes to other CMF shapes. Lastly, we note that the experimental data used in [Anklin et al., 2000] have not been reported with the publication.

5 CMF zero stability and repeatability

5.1 Zero-point stability

Emerson© product data sheet [Emerson, 2021] reports a zero stability of 0.47 kg/h for a CMF100 (delta shape) and of 1.30 kg/h for a CMF200 (U-shape). The percent error at the flow rate of interest is computed as

$$e_{zero} = \frac{\text{z.s.}}{Q} \cdot 100\,\% \,.$$

It is thus evident that the uncertainty contribution due to the zero stability is strongly dependent on the flow rate in use: the lowest the flow rate, the highest the relative error due to zero stability. Furthermore, it is thought that the zero stability will be more relevant in case of liquid hydrogen, since in this case boil-off is more likely to happen. However, there are no data available in this respect, so the best that can be done is to assume that the values obtained in case of liquid nitrogen or liquid natural gas are valid also for the case of liquid hydrogen. [Lucas et al., 2016] reported that at cryogenic conditions for liquid nitrogen and liquid natural gas the zero stability was $0.1\,\%$ in the worst case scenario for mass flow rate between 1 kg/h and 4 kg/h. Thus, a proxy of the standard uncertainty due to zero stability is estimated as $u_{zero} = 0.1\,\%/\sqrt{3} \approx 0.058\,\%$, assuming a uniform distribution for this error.

5.2 Repeatability

CMFs repeatability is difficult to measure since it is affected by the repeatability of the facility in which the flow meter is tested. Currently there are no liquid hydrogen facilities and there is no data regarding CMFs repeatability at liquid hydrogen temperatures. Due to the lack of information, we use the repeatability of a CMF200 calibrated at the VSL's LNG facility assuming that the CMF would behave in a similar fashion in case of liquid hydrogen. Thus we have $u_r = 0.018\,\%$ ($k = 1$) as a proxy for the CMF's repeatability.

6 Other uncertainties

6.1 Reynolds number

[Huber et al., 2013] and [Mills, 2020] show that CMF measurements present a dependency on the Reynolds number, which is particularly evident at low Reynolds numbers. They also note that compensation can be done

by measuring the viscosity of the fluid. Considering the typical range of Reynolds numbers that liquid hydrogen flow can reach, we should not worry about the dependency of the measurements on the Reynolds number.

6.2 Installation and velocity profile effects

CMFs are said to be insensitive to fluid properties [Costa et al., 2020], and independent from velocity profile and installation effects [Huber et al., 2013] (at least at first order). However [Levien, 1993] warns that external masses added to the tubing may interfere with the proportionality of frequencies (this can be corrected by adjusting the fixed masses), and that, because of secondary effects, reasonable tube vibration amplitude control is necessary.

More in detail studies using numerical simulations aiming to quantify the effect on CMF measurements due to velocity profiles and to installation effects have been performed. [Bobovnik et al., 2015] reported installation effects of $0.1\ \%$ for (modelled) twin tube flow meters using either a straight tube or curved U-tubes. However, the authors point out that the actual value of the installation effect for any specific configuration depends on the CMF's design features. Therefore, since this component is specific to each facility and each flow meter, and considering also the lack of data that could be used to validate such uncertainty estimate due to installation effects, we advise to take care during installation in order to avoid major effects and such that only minor (non-identifiable) installation effects are in place.

Regarding the magnitude of velocity profile effects [Kutin et al., 2006] concludes that this depends on many constructional and operational parameters of the CMF. Thus this effect seems to be very flow meter specific too and it will not be considered here in the uncertainty budget.

We note that both installation and velocity profile effects can be considered independent from the other uncertainty contributions discussed in this report and can thus be easily added to the total budget estimated here.

7 Uncertainty budgets

In table 1 the individual uncertainty components, their value and associated distributions are listed. For both the equation developed by Razsillier and Durst (1) and for the equation by Costa et al. (2) we use the Monte Carlo (MC) method to determine the combined uncertainty budget of all temperature related effects (i.e., Young's modulus, Poisson's ratio and thermal expansion). The resulting temperature related uncertainty component is then added to the uncertainty contributions due to pressure, zero stability and repeatability.

7.1 Monte Carlo simulations

We use the Monte Carlo method to propagate the uncertainties through equations (1) and (2). However the available equations allow to propagate only the temperature related uncertainties, while all the other contributions have to be added a-posteriori to the MC result. Since both equation (1) and (2) are valid for a U-shape CMF, here we compute an uncertainty budget for a U-shape meter, i.e. the CMF200 from Emerson©. The estimation of the uncertainty budget for a delta-shape CMF would first require validation of the available mass flow equation for this particular shape of CMF. However, since the only difference between a U-shape meter

Table 1: Uncertainty components of the total uncertainty budget of two (Emerson©) CMFs (a delta-shape and a U-shape CMF) at liquid hydrogen temperature after being calibrated with water. NA = Not Applicable.

Uncertainty component	Probability distribution	Standard uncertainty contribution (%)	
		CMF100	CMF200
Young's modulus	normal	0.5	0.5
Poisson's ratio	normal	MC	MC
Tube's thermal expansion coefficient	normal	0.008	0.008
Temperature measurement uncertainty effect on Young's modulus	uniform	0.042	0.042
Temperature measurement uncertainty effect on Poisson's ratio	uniform	MC	MC
Temperature measurement uncertainty effect on thermal expansion	NA	NA	NA
Pressure effect	normal	0.009	0.027
CMF zero stability	uniform	0.058	0.058
CMF repeatability (type A)	normal	0.018	0.018

and a delta-shape meter is the value of the pressure correction factor, we expect the procedure presented here to be easily applicable also to the case of a delta-shape CMF.

7.1.1 Uncertainty budget for a U-shape CMF200

We obtain the values of the geometrical parameters involved in the mass flow equations from the product data sheet [Emerson, 2021] and the technical data sheet [Emerson, 2019]. In case of an Emerson© U-shape CMF200 we have $L = 727$ mm, $W = 498$ mm, and $r_i = 26.9/2 = 13.45$ mm. However, we did not find any information regarding the outer diameter nor the thickness and therefore we assumed a thickness of 1.3 mm, as used by [Wu and Kenbar, 2022]. We run simulations using also different values for the thickness (e.g., 1.0 mm) and the results did not change significantly. We assigned a value equal to 1 p.d.u. (procedure defined unit) to all the constant values in the equations for which we did not find any specific value. Since we are interested in the relative difference with respect to the reference value, most constants cancel out when dividing the MC simulations results by the reference value. However these constant values act as multipliers of the differences caused by the uncertainties in E, ν and α, so it is advisable to use values as realistic as possible.

We used $n_{MC} = 1000000$ MC simulations where E and ν are drawn from $\mathcal{N}(207.8, 1.039)$ and $\mathcal{N}(0.282, 0.00141)$, respectively, where the means of the Gaussian distributions are the measurement values by [Ledbetter, 1981] at $T = 20$ K and the standard deviations are 0.5 % of the corresponding mean value. α is drawn from a normal distribution $\mathcal{N}(0.99696, 0.00008)$ and all other values involved in the equations are constant. The reference value is taken as the mean value over the MC simulations.

In figures 2 and 3 we show the relative deviations from the reference value,

$$\Delta Q_{rel} = \left(\frac{Q_{MC}}{\mathbb{E}[Q_{MC}]} - 1 \right) \cdot 100\%$$

where Q_{MC} is the result of a Monte Carlo simulation and $\mathbb{E}[Q_{MC}]$ is the mean value over the MC simulations.

The standard deviation of the so-defined deviations from the mean value are $u_{T,MC} \approx 0.500\,\%$ for the equation by Raszillier and Durst (1), and $u_{T,MC} \approx 0.556\,\%$ for the equation by Costa et al (2). These values can be considered as the overall uncertainty component due to temperature. To obtain the total uncertainty budget, we need to add the uncertainty due to pressure, the zero-point stability and repeatability to the MC result. Adding these additional contributions to the standard deviation obtained with the MC simulations according to the GUM returns $u_{Q_m,RD} \approx 0.504\,\%$ for the equation by [Raszillier and Durst, 1991] and $u_{Q_m,Costa} \approx 0.560\,\%$ for the equation by [Costa et al., 2020]. It can be easily noted that the major uncertainty source is the uncertainty in the measurements of the elastic properties of stainless steel.

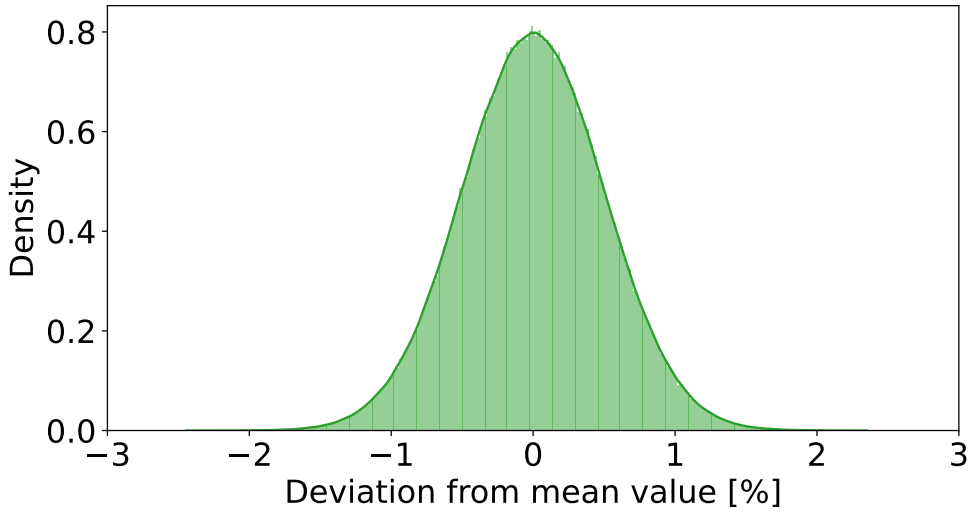

Figure 2: Distribution of relative difference between outcome of MC simulations and reference value using the equation by Raszillier and Durst (1) ([Raszillier and Durst, 1991]).

8 Conclusions

We reviewed the available literature on Coriolis mass flow meters and cryogenic measurements. In particular, we investigated the uncertainty in measurements of liquid hydrogen using a CMF calibrated with water.

We considered two physics-based equation for the mass flow through a CMF: one for a straight tube design and one for a U-shape meter. The equation for the straight tube has been validated also for a U-shape CMF. However, we did not find similar studies validating the equations for other CMF designs such as, e.g., a delta shape meter. Our research revealed that there is little information available on the behavior of the elastic modules of stainless steel at cryogenic temperatures. There is limited data available and their associated uncertainty is rather high. The total uncertainty in the Young's modulus of stainless steel 316 is $1.9\,\%$ (k=1) and (limited) information on the contribution of the individual uncertainty sources are available only for stainless steel 304. By assuming that the uncertainty budget for stainless steel 304 and 316 have been constructed in the same fashion and that the repeatability uncertainty reported for stainless steel 304 is valid also for stainless steel 316, we could reduce to $0.5\,\%$ both the uncertainty in the Young's modulus and in the Poisson's ratio. We remark that many uncertainty sources in the elastic properties are calibrated out in the water calibration

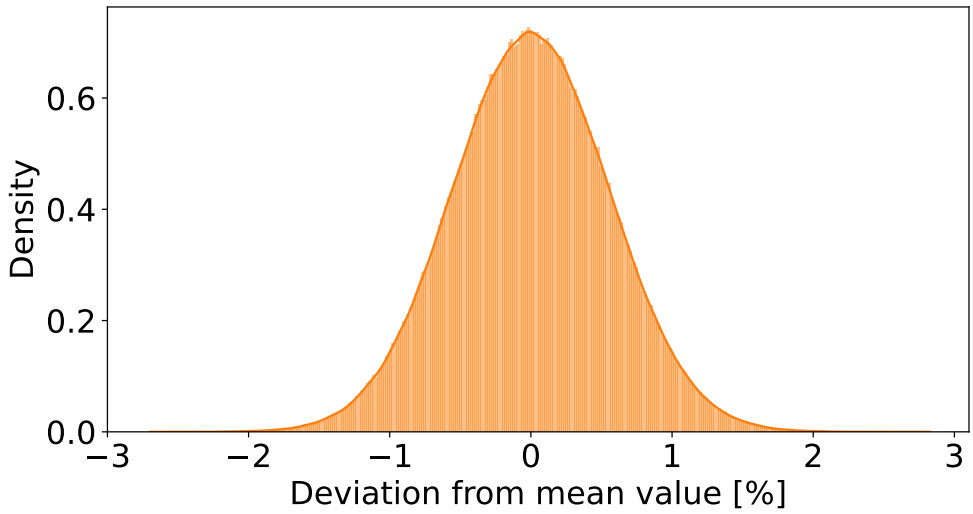

Figure 3: Distribution of relative difference between outcome of MC simulations and reference value using the equation by Costa et al. (2) ([Costa et al., 2020]).

and only the uncertainty at cryogenic temperatures and any measurement correlations need to be considered. However, this is not possible due to the limited amount of information available on the uncertainty budgets of the steel's elastic properties.

The results reported in the literature seem to agree that manufacturers have studied the effects of pressure on CMF measurements quite well, so that the uncertainty component due to pressure can be based on the pressure correction factor given by the manufacturers. The effect of measuring a two-phase fluid is still topic of active research. Some possible corrections have been formulated, but they have not yet been validated for CMF and for measurements at cryogenic temperatures. On the other hand, there is also active research meant to develop ways to store liquid hydrogen and reduce boil-off. Therefore, the error due to measuring a two-phase fluid might be different for each facility. Zero-point stability and repeatability also depend on the facility. Thus only proxies based on values for liquid natural gas and liquid nitrogen could be used, with the assumption that similar values are valid also for the case of liquid hydrogen. Finally, care should be taken when installing the flow meter to reduce the effects of the installation as much as possible, and if the flow has low Reynolds number, a correction can be made by measuring the viscosity of the fluid.

The uncertainty budget obtained by combining the different uncertainty sources is strongly dominated by the uncertainty in the Young's modulus and in the Poisson's ratio. This results in the need for more accurate data (and understanding) of the behavior of the elastic properties of stainless steel at cryogenic temperatures. The error caused by the presence of boil-off gas in the liquid also requires further investigation. However, given the large uncertainty associated with the elastic properties of the steel and the parallel research on improving storage of liquid hydrogen, we do not expect this error to be a major contributor to the uncertainty budget. In order to achieve more accurate measurements of the liquid hydrogen flow, we think that the priority should be to obtain more accurate information on the behavior of the elastic properties of the steel at cryogenic temperatures.

References

[Anklin et al., 2000] Anklin, M., Eckert, G., Sorokn, S., and Wenger, A. (2000). Effect of finite medium speed of sound on Coriolis massflowmeters. *Flomeko*.

[Aziz, 2021] Aziz, M. (2021). Liquid hydrogen: A review on liquefaction, storage, transportation, and safety. *Energies*, 14(18).

[Basse, 2014] Basse, N. T. (2014). A review of the theory of coriolis flowmeter measurement errors due to entrained particles. *Flow Measurement and Instrumentation*, 37:107–118.

[Basse, 2016] Basse, N. T. (2016). Coriolis flowmeter damping for two-phase flow due to decoupling. *Flow Measurement and Instrumentation*, 52:40–52.

[BIPM, 2008a] BIPM (2008a). Guide to the expression of uncertainty in measurements, JCGM 100:2008, GUM 1995 with minor corrections.

[BIPM, 2008b] BIPM (2008b). Supplement 1 to the guide to the expression of uncertainty in measurements - propagation of distributions using a Monte Carlo method.

[Bobovnik et al., 2015] Bobovnik, G., Kutin, J., Mole, N., Štok, B., and Bajsić, I. (2015). Numerical analysis of installation effects in coriolis flowmeters: Single and twin tube configurations. *Flow Measurement and Instrumentation*, 44:71–78.

[Büker et al., 2020] Büker, O., Stolt, K., de Huu, M., MacDonald, M., and Maury, R. (2020). Investigations on pressure dependence of Coriolis mass flow meters used at hydrogen refueling stations. *Flow Measurement and Instrumentation*, 76:101815.

[Costa et al., 2020] Costa, F. O., Pope, J. G., and Gillis, K. A. (2020). Modeling temperature effects on a Coriolis mass flowmeter. *Flow Measurement and Instrumentation*, 76:101811.

[Desai and Y., 1978] Desai, P. D. and Y., H. C. (1978). Thermal linear expansion of nine selected aisi stainless steels.

[Emerson, 2019] Emerson, M. M. (2019). Micro motion elite coriolis flow and density meters. Technical data sheet.

[Emerson, 2021] Emerson, M. M. (2021). Micro motion elite coriolis flow and density meters. Product data sheet.

[Hemp and Kutin, 2006] Hemp, J. and Kutin, J. (2006). Theory of errors in coriolis flowmeter readings due to compressibility of the fluid being metered. *Flow Measurement and Instrumentation*, 17(6):359–369. Coriolis Massflow Meters.

[Huber et al., 2013] Huber, C., Nuber, M., and Endress, M. (2013). Effect of Reynolds number in Coriolis flow measurement.

[Kuhny, 2011] Kuhny, D. (2011). Compensating for the effects of high pressure on the measurement accuracy of coriolis flowmeters.

[Kutin et al., 2006] Kutin, J., Bobovnik, G., Hemp, J., and Bajsić, I. (2006). Velocity profile effects in Coriolis mass flowmeters: Recent findings and open questions. *Flow Measurement and Instrumentation*, 17(6):349–358. Coriolis Massflow Meters.

[Ledbetter, 1980] Ledbetter, H. M. (1980). Sound velocities and elastic constants of steels 304, 310, and 316. *Metal Science*, 14(12):595–596.

[Ledbetter, 1981] Ledbetter, H. M. (1981). Stainless-steel elastic constants at low temperatures. *Journal of Applied Physics*, 52:1587–1589.

[Ledbetter et al., 1980] Ledbetter, H. M., Frederick, N. V., and Austin, M. W. (1980). Elastic-constant variability in stainless-steel 304. *Journal of Applied Physics*, 51(1):305–309.

[Levien, 1993] Levien, A. (1993). Basic principles for vibrating tube coriolis mass flow sensor design.

[Lucas et al., 2016] Lucas, P., Büker, O., Kenbar, A., Kolbjørnsen, H., Rasmussen, K., Rathwell, G., Safonova, M., Stolt, K., and van der Beek, M. P. (2016). World's first LNG research and calibration facility. *Flomeko*.

[Mills, 2020] Mills, C. (2020). Calibrating and operating Coriolis flow meters with respect to process effects. *Flow Measurement and Instrumentation*, 71:101649.

[NIST, 2017] NIST (2017). Material Properties: 316 Stainless. `https://trc.nist.gov/cryogenics/materials/316Stainless/316Stainless_rev.htm`. Online; accessed 2021-12-10.

[Raszillier and Durst, 1991] Raszillier, H. and Durst, F. (1991). Coriolis-effect in mass flow metering. *Archive of Applied Mechanics*, 61:192–214.

[Wang and Hussain, 2009] Wang, T. and Hussain, Y. (2009). Coriolis mass flow measurement at cryogenic temperatures. *Flow Measurement and Instrumentation*, 20(3):110–115.

[Wang and Hussain, 2010] Wang, T. and Hussain, Y. (2010). Pressure effects on Coriolis mass flowmeters. *Flow Measurement and Instrumentation*, 21(4):504–510.

[Wu and Kenbar, 2022] Wu, T. Y. and Kenbar, A. (2022). LNG mass flow measurement uncertainty reduction using calculated young's modulus and poisson's ratio for coriolis flowmeters. *Measurement*, 188:110413.

[Wu et al., 2021] Wu, T. Y., Kenbar, A., and Pruysen, A. (2021). LNG mass flowrate measurement using Coriolis flowmeters: Analysis of the measurement uncertainties. *Measurement*, 177:109258.

[Xu et al., 2020] Xu, X., Xu, H., Zheng, J., Chen, L., and Wang, J. (2020). A high-efficiency liquid hydrogen storage system cooled by a fuel-cell-driven refrigerator for hydrogen combustion heat recovery. *Energy Conversion and Management*, 226:113496.